GAS-SURFACE IMPACT ON AERODYNAMIC SURFACE QUANTITIES OF LOW-DENSITY HYPERSONIC FLOW OVER FLAT-NOSE BODIES

Wilson F. N. Santos
National Institute for Space Research
Combustion and Propulsion Laboratory
12630-000 Cachoeira Paulista, SP, Brazil
wilson@lcp.inpe.br

Abstract. The present work performs a computational study on rarefied hypersonic flow past flat-nose leading edges at zero incidence. Effects of incomplete surface accommodation on the aerothermodynamic surface quantities have been investigated by employing the Direct Simulation Monte Carlo (DSMC) method in combination with the Cercignani-Lampis-Lord gas-surface interaction model, which incorporates separate accommodation coefficients for normal and tangential velocity components. The work also focuses the attention of designers of hypersonic configurations on the fundamental parameter of bluntness, which can have an important impact on even initial design. The results presented highlight the sensitivity of the heat transfer and drag coefficients to changes on the gas-surface accommodation coefficients. These are compared to the results for classical diffuse reflection model. It was found that stagnation point heating decreased by a reduction on the normal accommodation coefficient and the total drag decreased by a reduction on the tangential accommodation coefficient.

Keywords: hypersonic flow, rarefied flow, DSMC, blunt leading edge, incomplete surface accommodation.

1. Introduction

Rarefied aerodynamic coefficients are determined by the transfer of momentum and energy during the interaction of incident molecules with the body surface. At the highest altitudes, the collisions between the incoming and reflected molecules can be neglected, and the regime is called free molecular flow regime. At lower altitudes, collisions between incoming molecules and reflected molecules as well as between incoming and the surface must be taken into consideration. This regime is called the transition flow regime. In this regime, the details of the gas-surface interaction process are also important, and the aerodynamic coefficients rely intimately on that process. Thus a knowledge of the interaction of incoming molecules with the surface of a vehicle is important for the accurate prediction of aerodynamic coefficients in the transition and free molecular flow regimes.

Currently, the Direct Simulation Monte Carlo (DSMC) method developed by Bird (1994) is the only viable technique for predicting the aerodynamics of bodies that pass through the transition regime and into the free molecular regime. The DSMC method requires knowledge of the velocity distribution function of the molecules that are reflected or re-emitted from the surface after they have collided with the surface. The most common gas-surface interaction model used in the DSMC calculations is the Maxwell model based on the classical thermodynamics. The Maxwell model assumes that molecules will either reflect specularly with no change in energy or will reflect diffusely from a surface with complete momentum and energy accommodation. The diffuse reflection model assumes that the molecules are reflected equally in all directions, quite independently of their incident speed and direction.

Nonetheless, as a space flight vehicle is exposed to a rarefied environment over a considerable time, a departure from the fully diffuse reflection model is observed, resulting from the colliding molecules that clean the surface of the vehicle that becomes gradually decontaminated. Molecules reflected from clean surface show lobular distribution in direction. The flux distribution of scattered molecules emitted from clean surface frequently has a lobular shape that is centered about an angle which tends to approach the specular angle for very high energies and/or low angle of attack. As a result, this flux distribution is poorly represented by the Maxwell model.

A phenomenological model that has demonstrated some improvement over the Maxwell model has been proposed by Cercignani and Lampis (1971). Their model contains separate adjustable accommodation coefficients for the kinetic energies associated with the normal and tangential components of velocity to the surface and produces more realistic distributions of velocity and direction of reflected molecules.

In the present work, the Cercignani-Lampis model is implemented into the DSMC method in order to investigate the sensitivity of the incomplete surface accommodation on the aerodynamic surface quantities of a rarefied hypersonic flow over flat-nose leading edges. Flat-nose leading edges have been considered (Santos 2003) as especially promising bluntness for hypersonic configurations, since they maintain bluntness necessary for heating control, manufacturing, and volume for active cooling.

2. Leading Edge Geometry

The blunt shapes consist of a flat nose supplemented by an afterbody surface defined, in dimensionless form, by the following contour,

$$\bar{x} = \int_{\bar{y}=1}^{\bar{y}=\bar{y}_{max}} \sqrt{\bar{y}^k - 1}\, d\bar{y} \qquad \text{where } \bar{x} = x/y_{nose} \text{ and } \bar{y} = y/y_{nose} \qquad (1)$$

The flat-nose shapes are modeled by assuming a sharp leading edge of half angle θ with a circular cylinder of radius R inscribed tangent to the wedge. The flat-nose shapes, inscribed between the wedge and the cylinder, are also tangent to them at the same common point where they have the same slope angle. The circular cylinder diameter provides a reference for the amount of blunting desired on the leading edges. It was assumed a leading edge half angle of 10 deg, a circular cylinder diameter of 10^{-2}m and flat-nose thickness t/λ_∞ of 0.01, 0.1 and 1, where $t = 2y_{nose}$ and λ_∞ is the freestream mean free path. Figure 1(a) illustrates this construction for the set of shapes investigated. From geometric considerations, the exponent k in Eq. (1) is obtained by matching slope on the wedge, circular cylinder and on the body shapes at the tangency point. For dimensionless thickness t/λ_∞ of 0.01, 0.1 and 1, k corresponds to 0.501, 0.746 and 1.465, respectively.
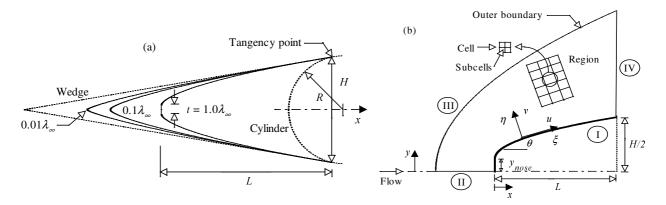

Figure 1: Drawing illustrating (a) the leading edge shapes and (b) the computational domain.

3. Computational Method and Procedure

The DSMC method has become today the most valuable technique for the investigation of rarefied gases. The DSMC method does not solve a system of equations to produce a solution of the flowfield, but rather statistically tracks movements and collisions of simulated molecules, each of which represents a fixed number of real gas molecules. In the movement phase, all particles are moved over distances appropriate to a short time interval, time step, and some of them interact with the domain boundaries in this time interval. Particles that strike the solid wall would reflect according to the appropriate gas-surface interaction model. In the collision phase, intermolecular collisions are performed according to the theory of probability without time being consumed. In this context, the intermolecular collisions are uncoupled to the translational molecular motion over the time step used to advance the simulation. Time is advanced in discrete steps such that each step is small in comparison with the mean collision time (Bird, 1994). The method does not require an initial approximation to the flowfield and there is no iterative procedure for convergence to the final solution.

The physical models employed in the present simulations are as follows. Intermolecular collisions are treated by using the variable hard sphere (VHS) molecular model (Bird, 1981) and the no time counter (NTC) collision sampling technique (Bird, 1989). Energy partitioning is accounted for using the Borgnakke-Larsen statistical model (Borgnakke and Larsen, 1975) with constant rotational and vibrational collision numbers, 5 for rotation and 50 for vibration.

In order to implement the particle-particle collisions, the flowfield is divided into an arbitrary number of regions, which are subdivided into computational cells. The cells are further subdivided into four subcells, two subcells/cell in each direction. The cell provides a convenient reference sampling of the macroscopic gas properties, whereas the collision partners are selected from the same subcell for the establishment of the collision rate.

The computational domain used for the calculation is made large enough so that body disturbances do not reach the upstream and side boundaries, where freestream conditions are specified. A schematic view of the computational domain is depicted in Fig. 1(b). Side I is defined by the body surface. Reflection with incomplete surface accommodation is the condition applied to this side. Advantage of the flow symmetry is taken into account, and molecular simulation is applied to one-half of a full configuration. Therefore, side II is a plane of symmetry. In such a boundary, all flow gradients normal to the plane are zero. At the molecular level, this plane is equivalent to a specular reflecting boundary. Side III is the freestream side through which simulated molecules enter and exit. Finally, the flow at the downstream outflow boundary, side IV, is predominantly supersonic and vacuum condition is specified (Bird, 1994). At this boundary, simulated molecules can only exit.

In order to simulate the partial surface accommodation, the Cercignani and Lampis (CL) model was implemented in

this DSMC calculation. Lord (1991) has shown that the CL model is suited for the DSMC method, and described how to incorporate it into the DSMC method. The DSMC method with Lord's implementation is referred as the Cercignani-Lampis-Lord (CLL) model. The CLL model is derived assuming that there is no coupling between the normal and tangential momentum components. The two adjustable parameters appearing in the CLL model are the normal component of translational energy α_n and the tangential component of momentum σ_t. expressed as being,

$$\alpha = \frac{e_i - e_r}{e_i - e_w} \qquad \sigma_t = \frac{\tau_i - \tau_r}{\tau_i} \qquad\qquad (2a, 2b)$$

where terms e and τ refer to the energy flux to the surface and the momentum flux acting tangential to the surface per unit area per unit time, respectively; subscripts i and r stand for the incident and reflected components, and w refers to the component that would be produced by a diffuse reflection at the temperature of the surface.

Numerical accuracy in DSMC method depends on the grid resolution chosen as well as the number of particles per computational cell. The effect of grid resolution on computed results is of particular interest for the present study because insufficient grid resolution can reduce significantly the accuracy of the predicted aerodynamic heating and forces acting on the body surface. Hence, heat transfer, pressure and skin friction coefficients are used as the representative parameters for the grid sensitivity. Grid independence was tested by running the calculations with half and double the number of cells in ξ and η directions (see Fig. 1(b)) compared to a standard grid. Solutions were near identical for all grids used and were considered fully grid independent. Due to the limited number of pages, the solutions will not be shown.

4. Flow Conditions

The freestream and flow conditions used in the present calculations are those given by Santos (2003) and summarized in Tab. 1. The freestream velocity V_∞, assumed to be constant at 3.56 km/s, corresponds to a freestream Mach number M_∞ of 12. The wall temperature T_w is assumed constant at 880 K, which corresponds to four times the freestream temperature.

Table 1: Freestream Conditions

Temperature T_∞ (K)	Pressure p_∞ (N/m^2)	Density ρ_∞ (kg/m^3)	Number density n_∞ (m^{-3})	Viscosity μ_∞ (Ns/m^2)	Mean free path λ_∞ (m)	Velocity V_∞ (m/s)
220.0	5.582	8.753 x 10^{-5}	1.8209 x 10^{21}	1.455 x 10^{-5}	9.03 x 10^{-4}	3560

The overall Knudsen number Kn_t, defined as the ratio of the freestream mean free path λ_∞ to the leading edge thickness t, corresponds to 1, 10 and 100 for leading edge thickness t/λ_∞ of 1, 0.1 and 0.01, respectively. The Reynolds number Re_t covers the range from 0.193 to 19.3, based on conditions in the undisturbed stream with leading edge thickness t as the characteristic length.

Finally, the DSMC calculations were performed independently for three distinct numerical values for α_n and σ_t: 0.5, 0.75 and 1. It is important to mention that α_n and σ_t equal to 1 represent the diffusion reflection.

5. Computational Results and Discussion

This section focuses on the effects that take place in the aerodynamic surface quantities due to variations on the normal and tangential accommodation coefficients as well as on the leading edge thickness. Aerodynamic surface quantities of particular interest in the transition flow regime are number flux, heat transfer, pressure, skin friction and drag. In this scenario, this section discusses and compares differences of these quantities expressed in coefficient form.

5.1. Number Flux

The number flux N is calculated by sampling the molecules impinging on the surface by unit time and unit area. The dependence of the number flux on the normal and tangential accommodation coefficients is illustrated in Figs. 2(a) and 2(b) for leading edge thickness t/λ_∞ of 0.01 and 1, that correspond to Kn_t of 100 and 1, respectively. In this set of figures, the dimensionless number flux stands for the number flux N normalized by $n_\infty V_\infty$, where n_∞ is the freestream number density and V_∞ is the freestream velocity. Also, S is the arc length s along the body surface measured from the stagnation point, normalized by the freestream mean free path λ_∞.

According to these plots, the dimensionless number flux to the surface depends not only on the leading edge thickness but also on the gas-surface interaction. For the sharp leading edge, Kn_t of 100 ($t/\lambda_\infty = 0.01$), the dimensionless

number flux is low and constant along the frontal surface and decreases gradually along the afterbody surface. Nevertheless, for the bluntest leading edge case investigated, Kn_t of 1 ($t/\lambda_\infty = 1$), the dimensionless number flux is large on the frontal surface. It presents a constant value in the first half of the flat face and decreases in the vicinity of the shoulder. After that, it decreases significantly along the afterbody surface. This increase in the dimensionless number flux with increasing the leading edge thickness may be related to the collisions of two groups of molecules; the molecules reflecting from the body and the molecules oncoming from the freestream. The molecules that are reflected from the body surface, which have a lower kinetic energy interact with the oncoming freestream molecules, which have a higher kinetic energy. Thus, the surface-reflected molecules collide again with the body surface, which produce an increase in the dimensionless number flux in this region. As expected, this behavior is less pronounced by a reduction on the normal or on the tangential accommodation coefficients, since the molecules are reflected from the surface with different energies. Consequently, the net buildup of particle density near the body surface is reduced.

Still referring to Figs. 2(a,b), it is apparent that the number flux is affected by a reduction on both accommodation coefficients. However, the manner in which the number flux is affected by the accommodation coefficients differs from sharp to blunt leading edges. Blunt leading edge, Kn_t of 1, is more affected by the normal accommodation coefficient whereas the sharp leading edge, Kn_t of 100, is more affected by the tangential accommodation coefficient.
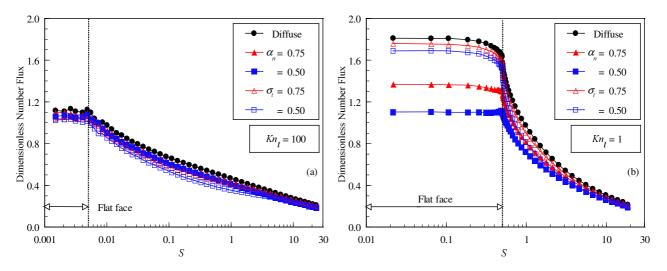

Figure 2: Dimensionless number flux ($N/n_\infty V_\infty$) along the body surface as a function of the partial accommodation coefficient for leading edges corresponding to Knudsen number Kn_t of (a) 100 and (b) 1.

5.2. Heat Transfer Coefficient

The heat transfer coefficient C_h is defined as being,

$$C_h = \frac{q_w}{\frac{1}{2}\rho_\infty V_\infty^3} \tag{3}$$

where q_w is the net heat flux to the body surface and ρ_∞ is the freestream density.

The heat flux q_w to the body surface is calculated by the net energy flux of the molecules impinging on the surface. A flux is regarded as positive if it is directed toward the surface. The net heat flux q_w is related to the sum of the translational, rotational and vibrational energies of both incident and reflected molecules as defined by,

$$q_w = q_i + q_r = \sum_{j=1}^{N} \left\{ \left[\frac{1}{2} m_j v_j^2 + e_{Rj} + e_{Vj} \right]_i + \left[\frac{1}{2} m_j v_j^2 + e_{Rj} + e_{Vj} \right]_r \right\} \tag{4}$$

where N is the number of molecules colliding with the surface by unit time and unit area, m is the mass of the molecules, v is the velocity of the molecules, e_R and e_V stand for the rotational and vibrational energies, respectively. Subscripts i and r refer to incident and reflected molecules.

Distribution of heat transfer coefficient along the body surface is plotted in Figs. 3(a,b) parameterized by the accommodation coefficient. Figures 3(a) and 3(b) illustrate C_h for thickness Knudsen number Kn_t of 100 and 1, respectively. It is noticed from Figs. 3(a,b) that the heat transfer coefficient is sensitive to the leading edge thickness as well as to the normal and tangential accommodation coefficients. The heat transfer coefficient remains essentially

constant over the front surface. Subsequently, the heat transfer coefficient decreases sharply and continues to decline along the body surface. However, for the bluntest case investigated, $Kn_t = 1$ ($t/\lambda_\infty = 1$), the heat transfer coefficient increases in the vicinity of the flat-face/afterbody junction.

Of particular interest is the behavior of the heat transfer coefficient in the vicinity of the flat-face/afterbody junction for the bluntest leading edge case. As the number of molecules impinging on the body surface decreases (see Fig. 2) in the vicinity of the leading edge shoulder, then the velocity of the molecules increases in this region in order to increase the heat transfer coefficient in this region. As a matter of fact, a molecular velocity rise in this region is expected due to the flow expansion along the shoulder of the leading edge.

It is also clearly seen in Figs. 3(a,b) that the heat transfer coefficient increases with decreasing the normal accommodation coefficient. In contrast, the heat transfer coefficient decreases with decreasing the tangential accommodation coefficient. An understanding of this opposite behavior can be gained by considering independently the contribution of the incident and reflected heat fluxes that appear in Eq. (4). In this scenario, Figs. 4(a,b) depict, respectively, the incident and reflected components of the heat flux for the $Kn_t = 1$ ($t/\lambda_\infty = 1$) case, in terms of the incident and reflected heat transfer coefficients.
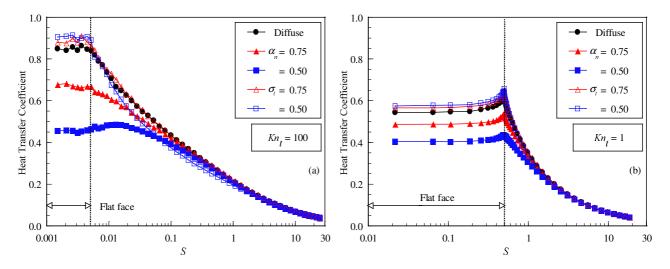

Figure 3: Heat transfer coefficient C_h along the body surface as a function of the surface accommodation coefficient for leading edges corresponding to Knudsen number Kn_t of (a) 100 and (b) 1.
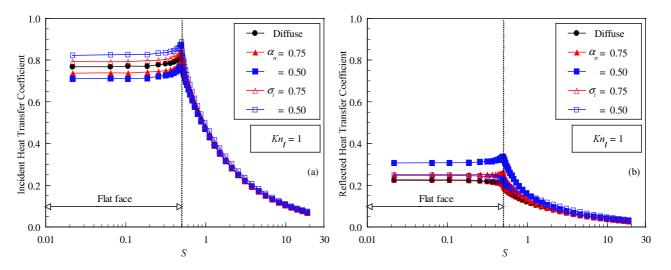

Figure 4: (a) Incident C_{hi} and (b) reflected C_{hr} heat transfer coefficients along the body surface as a function of the surface accommodation coefficient for the leading edge case corresponding to Knudsen number Kn_t of 1.

According to Fig. 4(a), it is observed that the incident heat flux contributes to increase the heat transfer coefficient along the frontal surface of the leading edge. With the reduction on the normal accommodation coefficient, the number flux was slightly reduced (see Fig. 2). In addition to that, the buildup of particle density near the body surface was slightly reduced (not shown), allowing the molecules oncoming from the freestream to transfer more energy to the body surface. Nevertheless, it is noticed from Fig. 4(b) that the reflected heat flux is almost identical as the normal

accommodation coefficient changes from 1 to 0.5. As a result, the net heat flux to the body surface is increased. On the other hand, the tangential accommodation coefficient exhibits an opposite behavior on the heat transfer coefficient. As one can see from Fig. 4, the incident heat transfer coefficient decreases and the reflected heat transfer coefficient increases as the tangential accommodation coefficient changes from 1 to 0.5. Consequently, a significant reduction is observed in the net heat flux to the body surface.

5.3. Pressure Coefficient

The pressure coefficient C_p is defined as being,

$$C_p = \frac{p_w - p_\infty}{\frac{1}{2}\rho_\infty V_\infty^2} \tag{5}$$

where p_w is the pressure acting on the body surface and p_∞ is the freestream pressure.

The pressure p_w on the body surface is calculated by the sum of the normal momentum fluxes of both incident and reflected molecules at each time step as follows,

$$p_w = p_i + p_r = \sum_{j=1}^{N} \left\{ \left[m_j v_{\eta j}^2 \right]_i + \left[m_j v_{\eta j}^2 \right]_r \right\} \tag{6}$$

where v_η is the normal velocity component of the molecules (see Fig. 1(b)).

The impact on pressure coefficient due to variations on the leading edge thickness and on the normal and tangential accommodation coefficients is demonstrated in Figs. 5(a,b). Figure 5(a) and 5(b) display, respectively, the pressure coefficient along the sharpest and the bluntest leading edges investigated, i.e, Kn_t of 100 and 1. It is worthwhile mentioning that the results for pressure coefficient as well as for the other surface quantities corresponding to the $Kn_t = 10$ ($t/\lambda_\infty = 0.1$) case have been leaved out because they are intermediate to the other cases shown.

Referring to Figs. 5(a,b), it is observed that the pressure coefficient distributions for the partial accommodation calculations are higher than those for full accommodation for the sharpest case ($Kn_t = 100$) investigated. In contrast, the partial accommodation calculations have no expressive effect on the pressure coefficient for the bluntest leading edge ($Kn_t = 1$).
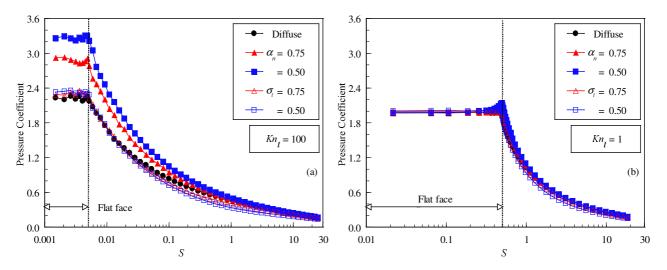

Figure 5: Pressure coefficient C_p along the body surface as a function of the surface accommodation coefficient for leading edges corresponding to Knudsen number Kn_t of (a) 100 and (b) 1.

In what follows, for convenience, the pressure coefficient is further evaluated in Figs. 6(a,b), that show, respectively, the contributions of incident and reflected components of the pressure coefficient along the body surface for the $Kn_t = 1$ ($t/\lambda_\infty = 1$) case. It is apparent from these plots that the energetic scattered molecules play a more significant role, since the incident component of the pressure coefficient decreases and the reflected one increases with decreasing the tangential accommodation coefficient. Hence, the insensitivity of the pressure coefficient to accommodation coefficient variations in the range investigated, shown in Fig. 5, is primarily attributed to a counterbalance between the number flux reduction and the tangential momentum rise related to the reflected molecules.
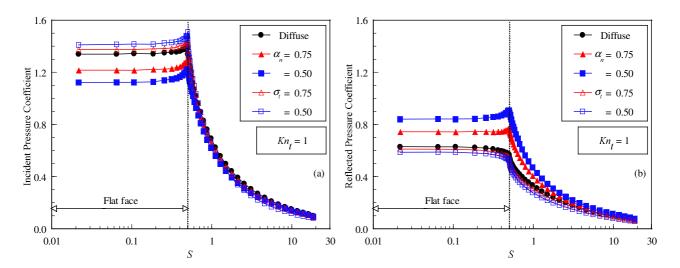
Figure 6: (a) Incident C_{pi} and (b) reflected C_{pr} pressure coefficients along the body surface as a function of the surface accommodation coefficient for the leading edge case corresponding to Knudsen number Kn_t of 1.

5.4. Skin Friction Coefficient

The skin friction coefficient C_f is defined as being,

$$C_f = \frac{\tau_w}{\frac{1}{2}\rho_\infty V_\infty^2} \tag{7}$$

where τ_w is the shear stress acting on the body surface.

The shear stress τ_w on the body surface is calculated by the sum of the tangential momentum fluxes of both incident and reflected molecules at each time step as follows,

$$\tau_w = \tau_i + \tau_r = \sum_{j=1}^{N} \left\{ \left[m_j v_{\xi j}^2 \right]_i + \left[m_j v_{\xi j}^2 \right]_r \right\} \tag{8}$$

where v_ξ is the tangential velocity component of the molecules (see Fig. 1(b)).

The variation of skin friction coefficient C_f with normal and tangential accommodation coefficient is depicted in Figs. 7(a) and 7(b) for Kn_t of 100 and 1, respectively. It is noted that the skin friction coefficient is zero at the stagnation point and slightly increases along the front surface up to the flat-face/afterbody junction of the leading edge.
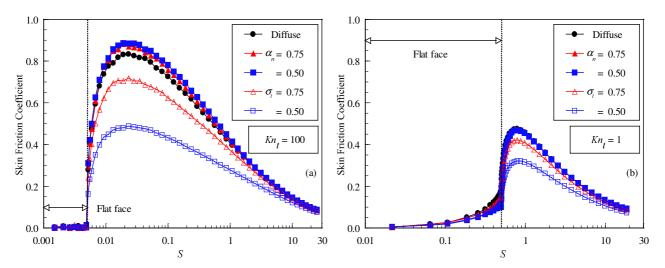

Figure 7: Skin friction coefficient C_f along the body surface as a function of the surface accommodation coefficient for leading edges corresponding to Knudsen number Kn_t of (a) 100 and (b) 1.

In the following, C_f increases dramatically to a maximum value that depends on the leading edge thickness, and decreases downstream along the body surface. Smaller thickness t (larger Kn_t) leads to higher peak value for the skin friction coefficient. Also, smaller thickness t displaces the peak value at the vicinity of the flat-face/afterbody junction. It is important to mention that the pick values for C_f in the afterbody surface occur at a station that corresponds to a body slope angle around 45 degrees (Santos, 2003). Of particular interest in Figs. 7(a,b) is the effect of the gas-surface interaction on the skin friction coefficient. As can be clearly seen, the skin friction is more sensitive to changes in the tangential accommodation coefficient than to changes in the normal accommodation coefficient.

It is important to mention that for the diffuse reflection model, reflected molecules have a tangential moment equal to zero, since the molecules essentially lose, on average, their tangential velocity component. In this connection, the second term in Eq. (8) is zero for diffusion reflection.

5.5. Drag Coefficient

The total drag coefficient C_d is defined as being,

$$C_d = \frac{F}{\frac{1}{2}\rho_\infty V_\infty^2 H} \tag{9}$$

where F is the resultant force acting on the body surface and H is the height at the matching point common to the leading edges (see Fig. 1(a)).

The drag force is obtained by the integration of the pressure p_w and shear stress τ_w distributions from the nose of the leading edge to the station L (see Fig. 1(a)), which corresponds to the tangent point common to all of the body shapes. In addition, the values for the total drag presented in this section were obtained by assuming the shapes acting as leading edges. Consequently, no base pressure effects were taken into account on the calculations.

Changes in the total drag coefficient C_d due to variations on the normal and tangential accommodation coefficients are displayed in Figs. 9 and 10, respectively. In this set of plots, the contributions of the pressure C_{pd} and skin friction drag C_{fd} to the total drag coefficient are also illustrated.

It is apparent from this set of diagrams that as the leading edge becomes blunter, i.e., the nose becomes flatter, the contribution of the pressure drag to the total drag increases and the contribution of the skin friction drag decreases, and the net effect results in a slightly increase in the total drag as the normal accommodation coefficient decreases from 1 to 0.5. In contrast, a considerable reduction in the total drag is observed with reducing the tangential accommodation coefficient. In this particular case, both pressure and skin friction drag contribute to reduce the total drag.
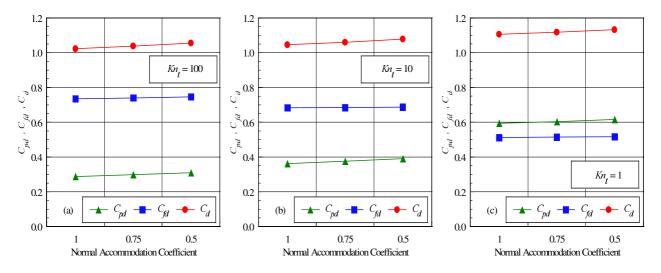

Figure 9: Pressure drag C_{pd}, skin friction drag C_{fd} and total drag coefficient C_d as a function of the normal accommodation coefficient for leading edges corresponding to Knudsen number Kn_t of (a) 100 and (b) 10 and (c) 1.

6. Concluding Remarks

The Direct Simulation Monte Carlo method is used to numerically simulate the rarefied hypersonic flow on blunt leading edges. The calculations provided information concerning the nature of the aerodynamic surface quantities for a family of contours composed by a flat nose followed by a highly curved afterbody surface. Effects of incomplete surface accommodation on the number flux, heat transfer coefficient, pressure coefficient, skin friction coefficient and

total drag coefficient for a range of normal and tangential accommodation coefficients are investigated. The normal and tangential accommodation coefficients are varied from 1.0 to 0.5, and the thickness of the frontal surface considered in this study covers hypersonic flow from the transitional flow regime to the free molecular flow regime.
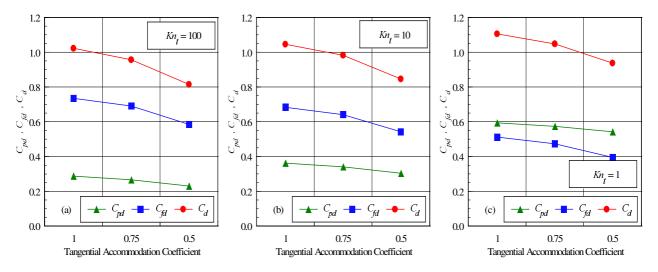

Figure 10: Pressure drag C_{pd}, skin friction drag C_{fd} and total drag coefficient C_d as a function of the tangential accommodation coefficient for leading edges corresponding to Knudsen number Kn_t of (a) 100 and (b) 10 and (c) 1.

Calculations showed that a reduction in the normal accommodation coefficient from 1.0 to 0.5 slightly increased the heat transfer coefficient in the vicinity of the stagnation point for the shapes investigated. In addition, it was found that a reduction in the tangential accommodation coefficient significantly diminished the heat transfer coefficient at the vicinity of the stagnation point for the leading edges investigated. Also, the analysis showed that the total drag coefficient is reduced by a reduction in the tangential accommodation coefficient, and increased by a reduction in the normal accommodation coefficient.

The effects of either normal or tangential accommodation coefficient showed that in order to make accurate predictions of the aerodynamic forces on, and heat transfer rates to, bodies in rarefied hypersonic flow it will be necessary to take surface accommodation into account. The calculations presented in this work have only covered a limited number of parametric variations. Further calculations with additional combinations of normal and tangential accommodation coefficients or where the internal energy accommodation is varied independently might provide more insight into the sensitivity of the aerothermodynamic quantities to gas-surface interaction model.

7. References

Bird, G. A., 1981, "Monte Carlo Simulation in an Engineering Context", Progress in Astronautics and Aeronautics: Rarefied gas Dynamics, Ed. Sam S. Fisher, Vol. 74, part I, AIAA New York, pp. 239-255.

Bird, G. A., 1989, "Perception of Numerical Method in Rarefied Gasdynamics", Rarefied gas Dynamics: Theoretical and Computational Techniques, Eds. E. P. Muntz, and D. P. Weaver and D. H. Capbell, Vol. 118, Progress in Astronautics and Aeronautics, AIAA, New York, pp. 374-395.

Bird, G. A., 1994, "Molecular Gas Dynamics and the Direct Simulation of Gas Flows", Oxford University Press, Oxford, England, UK.

Borgnakke, C. and Larsen, P. S., 1975, "Statistical Collision Model for Monte Carlo Simulation of Polyatomic Gas Mixture", Journal of computational Physics, Vol. 18, No. 4, pp. 405-420.

Cercignani, C. and Lampis, M., 1971, "Kinetic Models for Gas-Surface Interactions", Transport Theory and Statistical Physics, Vol. 1, No. 2, pp. 101-114.

Lord, R. G., 1991, "Application of the Cercignani-Lampis Scattering Kernel to Direct Simulation Monte Carlo Method", Proceedings of the 17th International Symposium on Rarefied Gas Dynamics, edited by A. E. Beylich, Aachen, Germany, pp. 1427-1433, July 8-14.

Santos, W. F. N., 2003, "Aerodynamic Heating on Blunt Nose Shapes in Rarefied Hypersonic Flow", Proceedings of the 17th International Congress of Mechanical Engineering, COBEM 2003, 10-14 Nov, São Paulo, SP, Brazil.